Experimental and theoretical studies of the $F+H_2$ transition state region via photoelectron spectroscopy of FH_2^-

Stephen E. Bradforth,[a] Don W. Arnold, and Daniel M. Neumark[b]
Department of Chemistry, University of California, Berkeley, California 94720 and Chemical Sciences Division, Lawrence Berkeley Laboratory, Berkeley, California 94720

David E. Manolopoulos
Department of Chemistry, University of Nottingham, Nottingham NG7 2RD, United Kingdom

(Received 25 May 1993; accepted 20 July 1993)

The transition state region of the $F+H_2$ reaction is studied by photoelectron spectroscopy of FH_2^-. The photoelectron spectra consist of overlapping electronic bands with different angular distributions. The ground state band shows partially resolved features which differ depending on whether the anion is made from *normal* or *para* hydrogen. This dependence on the anion nuclear spin statistics implies that these features are due to progressions in bending levels of the neutral FH_2 complex. In order to confirm this, and to determine the sensitivity of the photoelectron spectrum to the bend potential near the $F+H_2$ transition state, three-dimensional simulations of the FH_2^- photoelectron spectrum were performed assuming various potential energy surfaces for the $F+H_2$ reaction. We found that the London–Eyring–Polanyi–Sato surface proposed by Takayanagi and Sato gave better agreement than either the T5a or 5SEC surfaces. From the higher energy band, we can extract information on the $F+H_2$ excited electronic states, and several approximate simulations on model surfaces for these states are presented.

I. INTRODUCTION

This paper describes experimental and theoretical studies of the transition state region of the reaction $F+H_2 \rightarrow HF+H$ via photoelectron spectroscopy of the stable negative ion FH_2^-. The goal of this work is to combine experimental spectra with theoretical simulations in order to probe, in detail, the nature of the ground and excited state potential energy surfaces for the $F+H_2$ reaction in the vicinity of the transition state.

The $F+H_2$ reaction, along with its isotopic variants, has been one of the most thoroughly investigated reactions in chemical dynamics. Various aspects of the product energy and angular distributions have been measured in chemical laser,[1] infrared chemiluminescence,[2] and crossed molecular beam experiments.[3–5] Accurate rate constants have been obtained over a large temperature range.[6] From the theoretical perspective, interest in this reaction has centered on the development of accurate potential energy surfaces as well as the methodology to carry out detailed quantum mechanical reactive scattering calculations on these surfaces. Recent advances in scattering theory[7] now make it possible to compute detailed differential and integral reaction cross sections which, when compared to experiment, provide a stringent test for the various potential energy surfaces which have been proposed over the years.[8–13]

Although the interaction of a F atom with H_2 leads to three electronic states,[14] only the lowest of these is reactive, and most of the theoretical effort thus far has focused on this surface. The construction of a ground state potential energy surface which can reproduce all the experimental results has proved to be a challenge. The Muckerman 5 (M5) surface,[9] which was used in a series of scattering calculations prior to 1985,[15] matches the experimental HF vibrational distribution in classical trajectory calculations but not the rate constant or angular distribution. More recently, the dynamics of this reaction have been extensively investigated in quantal[16–22] and quasiclassical[23] scattering calculations using the T5a and 5SEC surfaces of Truhlar and co-workers,[10,11] both of which have considerably flatter bend potentials near the saddle point than the M5 surface. Calculations of the HF angular distributions[20,23] show that both surfaces approximately reproduce the experimental angular distributions.[4] However, while the experiments[1,2,4] show the HF ($v=2$) level is the dominant product vibrational channel, quantal calculations[20] on the T5a surface show HF ($v=3$) to be the most populated channel, and quasiclassical trajectory calculations[23] on the 5SEC surface predict approximately equal yields of HF ($v=3$) and ($v=2$). Hence these two surfaces apparently yield incorrect HF vibrational energy distributions. Another noteworthy surface is the empirical surface constructed by Takayanagi and Sato[12] (the TS surface). This does a reasonable job of reproducing both the experimental product energy and angular distributions in classical trajectory calculations, but the transition state theory rate constant on this surface is larger than the experimental value by a factor of 2.

What emerges from this body of work is that the calculated rate constant and product energy and angular distributions on a given surface have a complicated dependence on the height and location of the barrier as well as the bend potential near the barrier. This makes it difficult

[a]Present address: Department of Chemistry, University of Chicago, 5735 S. Ellis Avenue, Chicago, IL 60637.
[b]NSF Presidential Young Investigator, and Camille and Henry Dreyfus Teacher-Scholar.

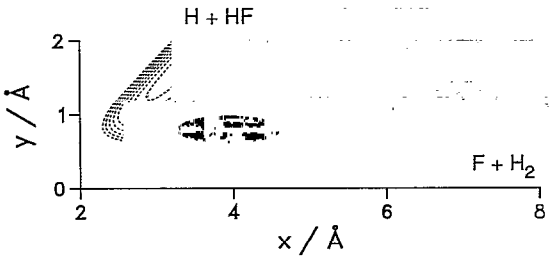

FIG. 1. Plot of F+H_2→HF+H ground state reaction surface with the FH_2^- ground vibrational state wave function shown shaded. The contours for the neutral potential surface are determined from the T5a potential function of Ref. 10. The saddle point (R_{F,H_2} = 1.953 Å, R_{H-H} = 0.762 Å) is marked with a cross. The anion wave function assumes the *ab initio* CCSD(T) equilibrium geometry (R_{F,H_2} = 2.075 Å and R_{H-H} = 0.770 Å) and MCSCF harmonic frequencies of Nichols *et al.* (Ref. 25); the ellipse represents the 90% probability limits of the wave function. The axes for the plot are mass scaled Jacobi coordinates: $x = (\mu_{F,H_2}/\mu_{H_2})^{1/2} R_{F,H_2}$ and $y = R_{H-H}$. The skew angle for FH_2 is 46°.

to "tweak" a particular region of a model surface in order to achieve better agreement with experimental results. Moreover, the exact calculation of state-resolved integral and differential cross sections on a given surface is quite lengthy,[20] as it involves summing over all the partial waves that contribute to the reaction.

In order to provide a more direct link between experiment and theory, and to provide experimental information complementary to that obtained from scattering experiments, we have performed a transition state spectroscopy experiment on the F+H_2 reaction via photoelectron spectroscopy of the stable negative ion FH_2^-. We have previously used this method to study several reactions, primarily involving the "heavy+light-heavy" mass combination.[24] This experiment provides a detailed probe of the "Franck–Condon region," the region of the neutral potential energy surface that has good geometric overlap with the negative ion. Figure 1 shows the ground state wave function of FH_2^-, based on the *ab initio* calculation by Nichols *et al.*,[25] superimposed on a collinear cut through the T5a F+H_2 surface. The Franck–Condon region clearly overlaps the saddle point, although more of its lies in the reactant valley than on the product side of the saddle point, so photodetachment of FH_2^- should probe the F+H_2 transition state region.

In our earlier photoelectron spectroscopy studies of this system,[26,27] we found that the photoelectron spectra of FH_2^-, FD_2^-, and FDH^- each consisted of two overlapping bands with markedly different photoelectron angular distributions. One band was assigned to a transition from the anion to the ground state F+H_2 surface, and the other to transitions to two additional low-lying excited electronic states that result from the interaction of $F(^2P)$ with H_2.[14] The ground state band showed partially resolved vibrational features which could be directly compared with simulations of the FH_2^- and FD_2^- photoelectron spectra by Zhang *et al.*[18,28] using the T5a surface. These are "exact" simulations which calculate the Franck–Condon overlap between the anion ground vibrational state (assuming total angular momentum J=0) and the three-dimensional scattering wave functions supported by the neutral potential energy surface. The experimental ground state band was found to be in qualitative agreement with the simulations (see below, however). Assignments of the partially resolved features in these spectra have been proposed by Hahn and Taylor,[29] using a classical analysis in which trajectories initiated in the Franck–Condon region were compared to periodic orbits,[30] and by Kress and Hayes,[22] who compared the peaks in the photoelectron spectrum to features in the quantum mechanical cumulative reaction probability.

This paper describes new experimental work in our laboratory, and an extensive new analysis of the FH_2^- photoelectron spectrum. Recent experimental improvements to our ion source have resulted in the production of colder anions, and the collection efficiency of our photoelectron detector has been increased, yielding higher signal-to-noise photoelectron spectra. Moreover, we report photoelectron spectra of FH_2^- made by clustering F^- with *para*-H_2, rather than with *normal*-H_2 as in our previous work. Our concern here was that in the latter case, the 75% of the H_2 molecules with j=1 (and higher odd values) were not rotationally quenched upon formation of the anion, leading to rotational and vibrational excitation of the anion. Indeed, the results reported here show that the photoelectron spectra obtained using *normal*- and *para*-H_2 are markedly different, and the implications for comparing the experimental and simulated spectra are discussed. New simulations of the FH_2^- spectra on several potential energy surfaces are also presented. The comparison with experiment shows that most of the resolved structure in the spectra is due to *bend* progressions in the neutral complex, and that the photoelectron spectrum provides an extremely sensitive probe of the bend potential near the saddle point.

The higher quality of the photoelectron spectra also allows us to analyze the excited state band, and to extract one-dimensional potential energy curves for the excited state interactions. These results are of interest in light of various calculations of the effects of the low-lying excited electronic states on reactive[31–35] and rotationally inelastic[36,37] F+H_2 scattering. The validity of this body of work is limited by the quality of the excited state potential energy surfaces used in the calculations; at the time, there were no experimental results to use as a check on the surfaces. Recently, Aquilanti *et al.*[38] extracted the long-range forms of the excited state potentials from total cross-section measurements using state-selected F atoms. The experimental results presented here provide the first quantitative determination of these surfaces at short range.

II. EXPERIMENT

The instrument employed in this study is the same time-of-flight photoelectron spectrometer described in our earlier work on FH_2^-.[26,27] Here we will describe only modifications to the experimental apparatus and the particular details of the experiments carried out. FH_2^- ions are made by crossing a pulsed free jet expansion of 8% NF_3/32% H_2/60% N_2 with a 1 keV electron beam. The presumed mechanism of ion formation is dissociative attachment to

NF_3 to form F^-, followed by clustering of the F^- with H_2 as the expansion progresses. A piezoelectric pulsed valve of the design of Proch and Trickl[39] was used in the work reported here; this was found to give cooler ions (i.e., the photoelectron spectrum is less congested and the features better resolved) than the General Valve pulsed valve used in our earlier studies. The addition of the N_2 in the reagent gas mixture was also found effective in cooling the ions. The gases are allowed to mix thoroughly in a stainless steel cylinder before use; at run time the stagnation pressure of the mixed gases behind the pulsed valve is 80 psig.

Ions are made from both *normal-* and *para*-hydrogen. The *normal*-H_2 (*n*-H_2) used in these experiments was obtained commercially and is 99.99% purity. The *para*-H_2 (*p*-H_2) was prepared by the University of California, Berkeley Department of Chemistry Low Temperature Laboratory, and is estimated to be 99.7% *p*-H_2 at the time of production. It was stored in standard aluminum gas cylinders in order to reduce *para–ortho* interconversion,[40,41] and used within a few hours of mixing with the other gases in the stainless steel mixing tank. While some interconversion may occur between generation of the *p*-H_2 and execution of the experiment, the significant differences observed between the photoelectron spectra of FH_2^- depending on whether *n*-H_2 or *p*-H_2 was used (see below) indicates that this interconversion was far from complete.

The negative ions are extracted, mass selected in a time-of-flight mass spectrometer, and photodetached with a pulsed Nd:YAG laser.[27,42] Spectra reported here were recorded using a laser wavelength of 266 nm (4.66 eV). The pulsed laser light is plane polarized; as before, we can adjust the angle θ between the electric vector of the laser radiation and the direction of electron detection by rotation of a half-wave plate. The second major change to our apparatus has been the upgrade of the electron detector. The electrons photodetached by the laser are detected at the end of a 1 m flight tube, and their energy is analyzed by time-of-flight. For this detector we now use a pair of 75 mm diam microchannel plates, rather than a pair of 40 mm plates.[42] This increases the electron collection efficiency by a factor of 3.5, with a similar improvement in the signal-to-noise. There is a slight loss in electron energy resolution due to the larger angular acceptance of the detector,[43] typically the instrumental resolution is 12 meV at 0.65 eV, and, as before, degrades for higher electron energies as $(eKE)^{3/2}$.

III. RESULTS

Photoelectron spectra were recorded for the FH_2^- ion made from *n*-H_2 and *p*-H_2 at two laser polarization directions, $\theta=0°$ and $\theta=90°$. The spectra are presented in Fig. 2. The form of the two *n*-H_2 spectra are similar to those reported earlier,[27] although more features are resolved at higher electron kinetic energy and there is a noticeable improvement in signal-to-noise in the $\theta=90°$ spectrum. The $\theta=90°$ spectrum consists of several partially resolved peaks between 0.8 and 1.1 eV, and a broad feature at lower electron kinetic energy. In the $\theta=0°$ spectrum, the peaks at higher kinetic energy are more intense, and the broad feature is largely suppressed. The partially resolved peaks at higher energy are labeled A, A′, B, C, and D in the $\theta=0°$ spectrum.[44] Peak A′ was not observed in our earlier spectrum, and peak C is better resolved here; both of these effects are attributed to lower ion temperatures in the current study.

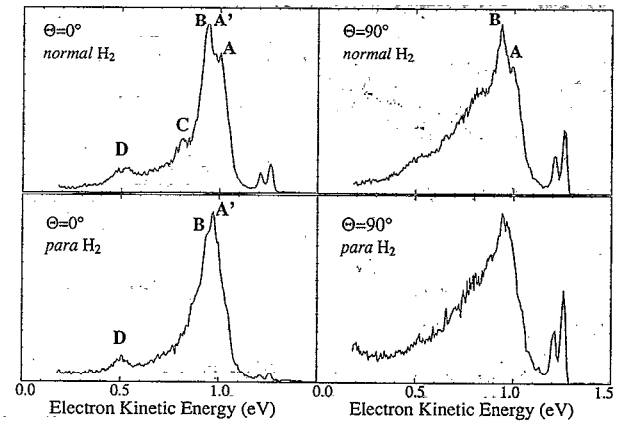

FIG. 2. Photoelectron spectra of FH_2^- at 266 nm. (Top) Ions made from *normal*-H_2 (3:1 *ortho/para*), and (bottom) ions made from *para*-H_2. Spectra recorded at two polarizations of the photodetachment laser: (Left) parallel [$\theta=0°$] and (Right) perpendicular [$\theta=90°$] to direction of electron collection.

The *p*-H_2 spectra in Fig. 2 show approximately the same dependence on laser polarization angle as the *n*-H_2 spectrum. However, the peaks between 0.8 and 1.1 eV appear markedly different in the *p*-H_2 spectrum, particularly the $\theta=0°$ spectrum. While the same peaks in the *n*-H_2 spectrum appear in the *p*-H_2 spectrum, the intensities are quite different. Peak A′ is the dominant feature in the *p*-H_2 spectrum, while peaks A and B, which appear cleanly in the *n*-H_2 spectrum, are barely observable shoulders on either side of peak A′ in the *p*-H_2 spectrum. Peak C is also less obvious in the *p*-H_2 spectrum and in its place a new shoulder seems to appear between B and C. Peak positions are listed in Table I.

The two peaks observed in all four spectra at 1.26 and 1.21 eV are due to a two photon process and correspond to the photoelectron spectrum of F^-, the first photon dissociates FH_2^- to F^-+H_2, the second photon detaches F^-.[27]

TABLE I. Peak positions (electron kinetic energies) in the $\theta=0°$, 266 nm photoelectron spectra of FH_2^-.

	Peak position/eV[a]				
FH_2^- from	A	A′	B	C	D
normal-H_2	1.000	0.972	0.941	0.815	0.54
para-H_2	0.996	0.970	0.942		0.51

[a]Peak positions in the table and in the spectra shown in Fig. 2 have been corrected for the small space charge shift (<5 meV) in the electron kinetic energies. Uncertainties in peak positions are 0.005 eV, except for peaks C and D where the uncertainty is approximately 0.015 eV.

IV. ANALYSIS AND DISCUSSION

A. Overview of spectrum and summary of previous analysis

The electron kinetic energy (eKE) is related to the initial energy of the anion, $E^{(-)}$, and the final energy of the neutral, $E^{(0)}$, by

$$\text{eKE}=h\nu-[D_0(FH_2^-)+\text{EA(F)}]-E^{(0)}+E^{(-)}. \quad (1)$$

Here EA(F)=3.401 190 eV is the electron affinity of atomic fluorine,[45] and $D_0(FH_2^-)$ is the dissociation energy of the anion to form $F^-+H_2(v=0)$; the *ab initio* value of D_0 is 0.20±0.10 eV.[25] Equation (1) shows that transitions at lower electron kinetic energy typically correspond to higher energy states of the neutral. In contrast, simulations of the photoelectron spectrum presented below are typically plotted as a function of the scattering energy E, defined with respect to the bottom of the F+H_2 well at infinite reactant separation, so that

$$E=E^{(0)}+zpe(H_2). \quad (2)$$

The differences in the photoelectron spectra at laser polarizations $\theta=0°$ and $\theta=90°$ indicate that there are two types of transitions in the spectra with markedly different photoelectron angular distributions. This implies that the two types of transitions are from different anion→neutral electronic transitions. On this basis, we previously assigned peaks A–D in the n-H_2 spectrum to transitions to the ground state F+H_2 potential energy surface, and the broad feature at lower electron energy, particularly prevalent in the 90° spectra, to transitions to the two low-lying excited state surfaces. In addition, peaks A–D shifted upon isotope substitution in the anion and were therefore assigned to vibrational features associated with the ground state F+H_2 surface. Peaks A–C occur at electron kinetic energies just below the F+$H_2(v=0)$ asymptote at eKE =1.06 eV (i.e., the eKE corresponding to $E^{(0)}=0$, assuming $D_0=0.20$ eV); according to Eq. (1), these peaks correspond to levels of the FH_2 complex that lie slightly above this asymptote. The more specific assignment of these peaks is discussed below. Peak D is separated from the centroid of peaks A, A′, and B by about one H_2 vibrational quantum and apparently corresponds to a level that correlates to F+$H_2(v=1)$; this assignment is supported by the isotopic substitution results.[27]

In the following sections, we first focus on the ground state transitions, particularly the differences between the n-H_2 and p-H_2 spectra. A comparison of these results to new simulations on several proposed F+H_2 surfaces offers a convincing assignment of the features in the photoelectron spectrum. We then analyze the excited state transitions and compare the excited state potential energy curves extracted by our analysis to those obtained by Aquilanti *et al.*[38]

B. Nuclear spin statistics in the anion and its effect on the photoelectron spectrum

The differences between the FH_2^- photoelectron depending on whether n-H_2 or p-H_2 is used to make the anion

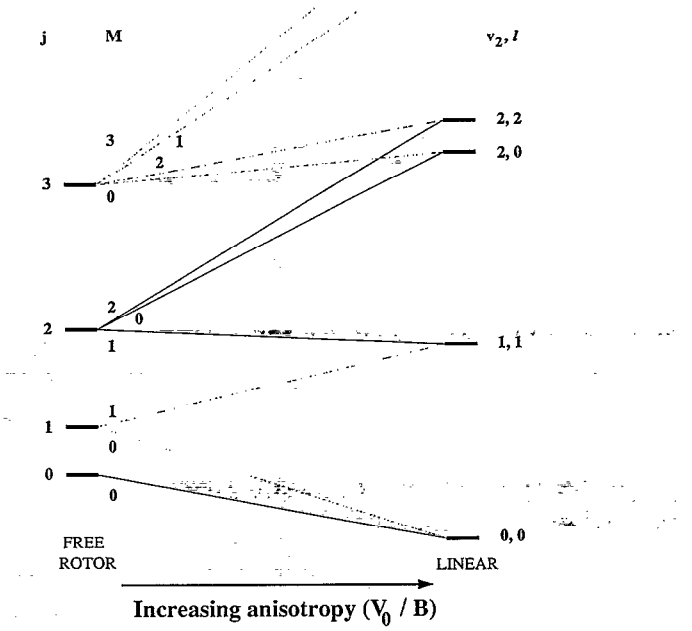

FIG. 3. Correlation diagram for bend/hindered rotor energy levels of FH_2^-. Labels j and M correspond to the free rotor total angular momentum and its projection on the body fixed axis; v_2 and l are the vibrational quantum number and the vibrational angular momentum for the degenerate linear bend. The solid lines indicate vibrational states that are symmetric with respect to H nuclei permutation, the dashed lines for antisymmetric states. Figure adapted from that for Ar..O_2 from Ref. 47.

demonstrate that the spin state of the H_2 has a marked effect on the photoelectron spectrum. As the H–H bond is not broken when the weakly bound FH_2^- anion is formed, the nuclear spin state of the H_2 must be preserved in the anion. Hence, we can refer to two distinct anion species, p-FH_2^- and o-FH_2^-, depending on whether the anion contains a *para*- or *ortho*-H_2 moiety. The anion spin statistics can lead to two interesting effects in the photoelectron spectrum. First, different manifolds of internal states are associated with p-FH_2^- and o-FH_2^-. Second, photodetachment of the two forms of FH_2^- accesses two distinct sets of scattering states in the neutral, namely, the states whose scattering wave function is symmetric with respect to permutation of the H nuclei (*para* states) and those that are antisymmetric (*ortho*). For example, scattering states that are symmetric with respect to hydrogen permutation are those that correlate to F+H_2 (j=even). We now consider both of these effects in more detail.

FH_2^- is predicted to have a linear equilibrium geometry,[46] and the relationship between the nuclear spin symmetry and the bending/hindered rotor mode of the anion can be understood using the correlation diagram in Fig. 3. This diagram derives from work by Henderson and Ewing on Ar–O_2 and Ar–N_2 complexes,[47] and shows how the hindered rotor levels near the free rotor limit transform to bending levels in the rigid linear molecule limit. In the free rotor limit, as for free H_2, the *para* form exists only in even j states, where j is the internal rotor quantum number, and the *ortho* form of the triatomic only in odd j states. In the rigid bender limit, the energy levels become identical to those of a degenerate harmonic oscillator. However, there

is a doubling of each state due to the two equivalent positions of the H nuclei. For each state there is a pair of wave functions: one is symmetric (s) and the other antisymmetric (a) with respect to permutation of the H nuclei. Near the rigid bender limit, with a large but finite barrier to internal rotation of H_2 in the complex, the symmetric and antisymmetric levels split as indicated in Fig. 3. For the purposes of our experiment, the relative proportions of symmetric to antisymmetric states of FH_2^- reflect the ratio of *para-* to *ortho*-hydrogen used in the clustering process, irrespective of what the actual value of V_0/B may be. Therefore *para*-H_2 will form only even symmetry states of FH_2^- shown in Fig. 3; *normal*-H_2 will form 1:3 symmetric to antisymmetric states.

We have performed *ab initio* calculations[48] on FH_2^- that indicate the barrier to internal rotation of the H_2 is about 3000 cm^{-1}; this agrees with recent higher level calculations by Simons.[49] Such a barrier is substantially larger than the rotational constant of H_2, 60 cm^{-1}, implying that the FH_2^- energy levels lie near the rigid bender limit. The splitting between the symmetric and antisymmetric levels associated with a bend level of the anion should then be small compared with the bend frequency (calculated value, ω_2=773 cm^{-1}).[25] Thus, if only the ground bend levels were populated in *p*-FH_2^- and *o*-FH_2^-, the small splitting between the symmetric and antisymmetric levels is not likely alone to be the cause of the difference between the *p*-FH_2^- and *n*-FH_2^- photoelectron spectra.

On the other hand, Fig. 3 shows that the $F^-/H_2(j=1)$ free rotor state formed from F^- with $H_2(j=1)$ correlates partially to the antisymmetric $v_2=1$ bend level of FH_2^-, while the $F^-/H_2(j=0)$ free rotor state correlates only to the ground vibrational state of FH_2^-. One might therefore expect more bend-excited FH_2^- to be formed when *n*-H_2 is used than when *p*-H_2 is used (assuming efficient rotational cooling of the *p*-H_2 to $j=0$ prior to clustering with the F^-). This represents a significant amount of internal energy which would certainly be expected to affect the photoelectron spectrum. However, the actual population of the antisymmetric $v_2=1$ level will depend on how much subsequent cooling to the antisymmetric $v_2=0$ level occurs in the free jet expansion. The similarities between the rising edges (at high eKE) of the *n*-FH_2^- and *p*-FH_2^- photoelectron spectra, where hot band effects should be most noticeable, suggest that cooling of the bending mode is quite effective.

A more likely explanation of the difference between the *n*-FH_2^- and *p*-FH_2^- spectra lies in the neutral scattering states accessible from photodetachment of the symmetric and antisymmetric levels of the anion. A correlation diagram similar to Fig. 3 can be applied to the *neutral* hindered rotor/bend levels in the entrance valley of the F+H_2 potential energy surface. Figure 3 applies only if the system is collinear in the rigid limit; a similar diagram[47] shows how free rotor levels correlate to the vibrational levels of a bent A_2B molecule. In any case, the recent surfaces proposed for the reaction have fairly flat bend potentials in the Franck–Condon region so, in contrast to the anion, we expect the neutral levels to lie considerably closer to the free rotor limit. Since the nuclear spin symmetry is unchanged by photodetachment, photodetachment of symmetric anion levels can only access symmetric neutral levels, and similarly for the antisymmetric levels. Hence, the photoelectron spectrum of *p*-FH_2^- can consist of progressions only in symmetric hindered rotor/bend levels of the neutral complex, that is, levels that correlate to F+H_2 (j even), while the *n*-FH_2^- spectrum can have progressions in both antisymmetric and symmetric levels, with a 3:1 preference for the former. The notion that it is the different manifolds of accessible neutral scattering states which are responsible for the differences between the two photoelectron spectra is strongly supported by the simulations discussed in the next section.

C. Comparison of experimental and simulated photoelectron spectra

1. Theoretical methodology

The exact simulation of anion photoelectron spectra as Franck–Condon factors between bound anion vibrational wave functions and neutral reactive scattering wave functions was pioneered by Schatz[50,51,52] and Zhang and Miller.[18] Because these Franck–Condon factors only require reactive scattering wave functions with total angular momentum $J=0$, at least to a good first approximation, they are relatively easy to compute using any one of a number of exact quantum reactive scattering methods.

The new FH_2^- simulations reported in the present paper were performed using a coupled-channel Delves hyperspherical coordinate method similar to the one described by Schatz.[53] However, in contrast to the method chosen by Schatz to study the photoelectron spectra of $ClHCl^-$[50] and IHI^-,[51] the required Franck–Condon overlaps with the ground FH_2^- vibrational wave function were accumulated directly during the coupled-channel integration without explicitly calculating reactive scattering wave functions. This was done by using a hyperspherical coordinate version of the driven equation formulation of Band *et al.*[54] in conjunction with an improved log derivative propagation algorithm.[55] A simple way to implement the solution of driven close-coupled equations using the log derivative method has recently been described elsewhere.[56]

The ground vibrational wave function of *para*-FH_2^- was modeled as a symmetrized product of harmonic normal mode wave functions, as described in the paper by Zhang and Miller.[18] The ground vibrational wave function of *ortho*-FH_2^- was modeled as the corresponding antisymmetrized product, and the appropriate H_2 permutation symmetry block of the F+H_2 reactive scattering problem was selected accordingly for each simulation. The coupled-cluster (CCSDT) anion equilibrium geometry (R_{F,H_2} = 2.075 Å, r_{H-H} = 0.770 Å) and multiconfiguration self-consistent-field (MCSCF) anion vibrational frequencies (ω_1=292 cm^{-1}, ω_2=773 cm^{-1}, ω_3=4143 cm^{-1}) were taken from the *ab initio* calculations of Nichols *et al.*[25]

Finally, in order to facilitate doing a large number of calculations of comparable accuracy on several different

$F+H_2$ potential energy surfaces, the input to our Franck–Condon factor program was streamlined. This was accomplished by using a series of one-dimensional heuristics to reduce the quadrature rule and basis set parameters required by the reactive scattering part of the program to two simple input parameters E_{max} and j_{max}.[19] (The most obvious roles of these parameters are that E_{max} is a cutoff for the energy, and j_{max} is a cutoff for the diatomic rotational quantum number, of the asymptotic channels that are retained in the calculation.) These two parameters were then increased for each separate calculation until the results were converged to graphical accuracy. The resulting optimum production parameters were typically $j_{max}=17$ and $E_{max}=1.7$ eV, measured from the bottom of the $F+H_2$ valley. Similar parameters have also been found to give well-converged results for $F+H_2$ reactive scattering at an energy of $E=0.45$ eV,[19] which lies above the dominant peaks in the simulated FH_2^- spectra.

2. T5a surface

In previous work, the photoelectron spectrum of *n*-FH_2^- was compared with the simulation by Zhang *et al.*,[18,28] in which the T5a surface was used for the neutral reaction. The anion was assumed to lie at the rigid bender limit, and the simulations used preliminary *ab initio* equilibrium parameters for the anion calculated by Nichols *et al.*[25,57] However, Zhang and Miller explicitly chose the anion ground state wave function to be symmetric with respect to nuclear exchange,[18] so Frank–Condon overlaps were computed with only the symmetric set of scattering states. In fact, their calculation employs a separation of the scattering problem by nuclear inversion symmetry,[58] and only one block, the *para* block, is used in the Franck–Condon calculation. Thus, the appropriate comparison with experiment is with the *para*-FH_2^- spectrum, *and not with the normal-FH_2^- spectrum* as previously done.[27,28] This only becomes an issue in light of the new experimental results showing that the *p*-FH_2^- and *n*-FH_2^- spectra are different.

Figure 4(a) shows the correct comparison of the T5a simulation of the FH_2^- photoelectron spectrum with our *para*-FH_2^- results. In this figure, we use $D_0=0.23$ eV for the dissociation energy of $FH_2^-(v=0)$ to $F+H_2(v=0)$, since this aligns the most intense peaks in the experimental (peak A′) and simulated spectra, as well as the smaller peaks at 0.5 eV. This value is well within the range of the *ab initio* value of Nichols (0.20 ± 0.10 eV), but is slightly smaller than the value used in our previous comparison of the simulation with the *n*-FH_2^- spectrum (0.26 eV).

The *normal*-FH_2^- spectrum, in contrast, contains transitions that are 75% due to antisymmetric states. Therefore, to simulate this photoelectron spectrum, a computation of the anion overlap with *ortho* scattering wave functions should be made and then added to the *para* simulation shown in Fig. 4(a) in the correct ratio. We have recently carried out exactly this calculation, using the method in Sec. 4C 1. In these calculations, we have first reproduced Zhang and Miller's result for *para*-FH_2^-, and then gone on to compute the *ortho* scattering states and their Franck–Condon overlap with the antisymmetrized anion ground state wave function, which, in the rigid bender limit, is at the same energy as the symmetric wave function. Together these simulations yield the theoretical photoelectron spectrum of *normal*-FH_2^- shown in Fig. 4(b), where it is compared to the experimental *normal*-FH_2^- spectrum.[59]

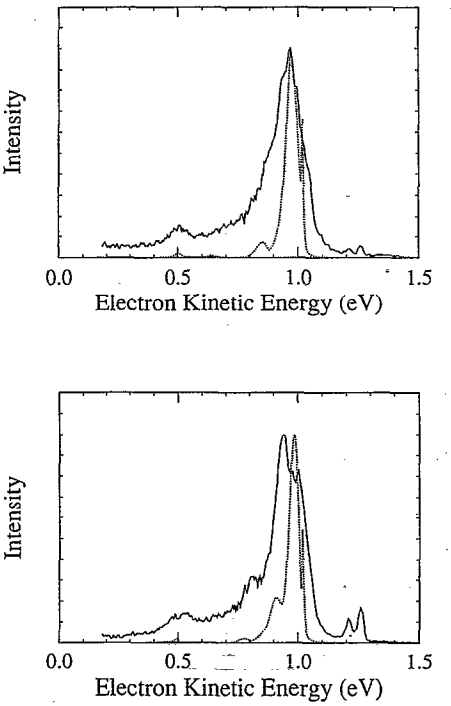

FIG. 4. [(a), top] Three-dimensional simulation (dotted) of the FH_2^- photoelectron spectrum using the T5a surface, considering only symmetric permutation states, of Zhang and Miller (Ref. 28) compared to $\theta=0°$ FH_2^- (*para*-H_2) experimental spectrum (solid). [(b), bottom] Three-dimensional simulation (dotted) of the FH_2^- photoelectron spectrum, considering both symmetric and antisymmetric permutation states compared to the $\theta=0°$ FH_2^- (*normal*-H_2) experimental spectrum (solid). The simulation is a weighted sum of the *p*-FH_2^- and *o*-FH_2^- simulations. Both calculations assume the same anion and neutral parameters and $D_0(F^-..H_2)=0.23$ eV (see the text).

Figures 4(a) and 4(b) make two points. First of all, although the energy of the initial anion state is the same in the *para* and *ortho* Franck–Condon calculations, the simulations are noticeably different, supporting the idea that the overlap with different sets of scattering states is responsible for the differences in the photoelectron spectra. Second, the overall comparison of the experimental and simulated spectra is not as good as was originally believed when the *n*-FH_2^- spectrum was first compared to the *para* simulation.

This is partly because of the new value of D_0 for FH_2^- used to achieve the best fit between the *p*-FH_2^- experimental and simulated spectra; the new value shifts the simulated spectra 0.03 eV towards higher electron kinetic energy. In addition, the spacings of features in the simulations are clearly inconsistent with the experimental spacings given in Table I; the eKEs of the four most intense peaks in the simulation are 1.018, 0.972, 0.852, and

0.502 eV. Also, peak A in the experiment *n*-FH_2^- spectrum was originally believed to correspond to the sharp peak just above 1.0 eV in the *para* simulation. While this peak is more intense in the *n*-FH_2^- experimental spectrum than in the *p*-FH_2^- spectrum, it is less intense in the *normal* simulation compared to the *para* simulation. This indicates that the original correspondence inferred by us was fortuitous. This is an important point, because the analysis of the cumulative reaction probability[22] on the T5a surface shows that the sharp peak in the simulation is from a reactive resonance. Based on the new results, this particular resonance is not apparent in the experiment.

Overall, Fig. 4 shows that simulations on the T5a surface do not reproduce key features of the experimental spectrum. This suggests that simulations on other potential energy surfaces proposed for the $F+H_2$ reaction would be useful, and these are discussed in the next section.

3. Simulations on the 5SEC and TS surfaces

In this section, we consider simulations on two additional $F+H_2$ surfaces: the 5SEC surface proposed by Lynch *et al.*[11] and the TS surface proposed by Takayanagi and Sato.[12] The 5SEC surface is based on an *ab initio* surface which is improved near the saddle point using "scaled external correlation," [60] and which also incorporates long-range attractive terms in the potential that result in a shallow van der Waals well in the reactant valley. The TS surface is a purely empirical modified London–Eyring–Polanyi–Sato[61] (LEPS) surface which approximately reproduces the experimental angular distributions[4] and HF vibrational population distribution[1,2,4] in classical trajectory calculations. The bend potentials for the three surfaces at their saddle points are shown in Fig. 5. These are plotted as a function of the Jacobi angle γ, defined in Fig. 5. The bend potentials are all quite flat, but the other two surfaces favor bent geometries at the transition state to a greater extent than the T5a surface.

Figures 6 and 7 show simulated spectra obtained using the 5SEC and TS surfaces. These again assume the anion is in the rigid bender limit, and use the *ab initio* anion geometry and frequencies of Ref. 25. Figures 6(a) and 7(a) are *para* simulations, and Figs. 6(b) and 7(b) are *ortho* simulations [antisymmetric wave functions only, unlike Fig. 4(b)]. Note that these simulations are plotted as a function of scattering energy *E*, related to the electron kinetic energy by Eqs. (1) and (2). Table II lists the energies and widths of the peaks in these simulations. A comparison of Figs. 4(a), 6(a), and 7(a) shows that the simulations are extremely sensitive to the potential energy surface assumed for the reaction; the peak spacings, intensities, and widths are very different in the three simulations. Moreover, the differences between the *para* and *ortho* simulations on the 5SEC and TS surfaces are even more pronounced than on the T5a surface.

There appear to be two types of peaks in the simulations: those that appear in both the *para* and *ortho* simulations and those that do not. The former are numbered, and the latter are labeled with capital letters. (Note that these letters are not intended to correspond to the experimental peaks in Fig. 2). The above discussion suggests that the lettered peaks appearing only in the *para* simulations are due to transitions to symmetric bend/hindered rotor levels of the FH_2 complex, while those peaks that appear only in the *ortho* simulations correspond to antisymmetric levels. The 5SEC simulations can be compared to the $F+H_2$ ($j=0$) cumulative reaction probability (CRP) calculated by Kress and Hayes[22] on the 5SEC surface (with total $J=0$). Peaks A, B, and C in the simulation occur at very nearly the same energy as steps A, B, and C in their CRP. These steps correspond to vibrational levels of the transition state becoming accessible,[62] and the comparison with the simulated photoelectron spectra implies these transition state levels are symmetric bend levels of the FH_2 complex. Peaks D and E do not appear in Kress calculation. This is consistent with our interpretation, since antisymmetric bend levels would not be accessible from $F+H_2$ ($j=0$) reactants.

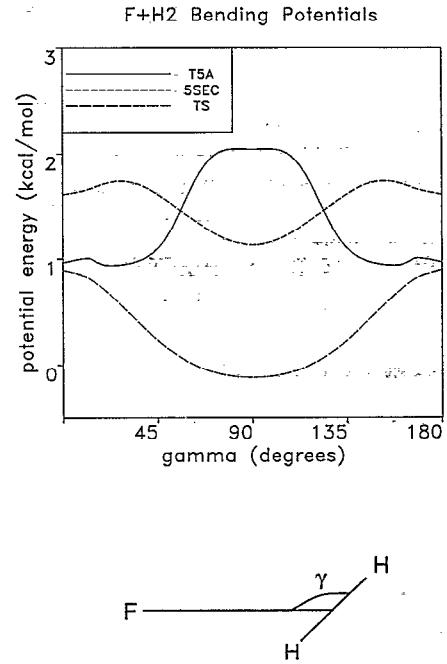

FIG. 5. Plot of bend potentials at the saddle point for the T5a, 5SEC, and TS potential energy surfaces as function of Jacobi angle γ, defined in lower half of the figure.

Peaks 1 and 2 do not correspond to any features seen in $F+H_2$ reactive scattering calculations on the 5SEC surface. In fact, both occur at energies below the threshold for reaction on this surface ($\sim$0.30 eV),[21,22] and peak 1 lies below the reactant zero-point energy (0.269 eV). This suggests that both peaks correspond to scattering states which are localized on the H+HF side of the saddle point. Such states are accessible via photodetachment, provided they have sufficient overlap with the anion, but do not appear in $F+H_2$ scattering calculations (or experiments!). This assignment is supported by simulations which assume a larger R_{F,H_2} distance for the anion (2.377 vs 2.074 Å, not shown); peaks 1 and 2 are virtually absent in these simulations, while the lettered peaks are of comparable inten-

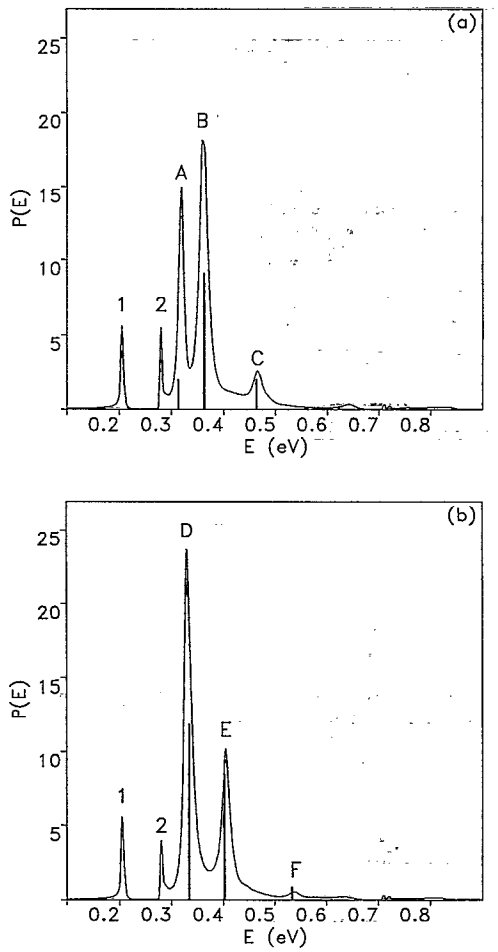

FIG. 6. (a) Three-dimensional simulations of *para*-FH_2^- spectrum on 5SEC surface for F+H_2. One-dimensional simulation (see the text) is superimposed as stick spectrum. For ease of comparison, the one-dimensional intensities are scaled so that the most intense one-dimensional peak is half the height of the most intense three-dimensional peak. Simulations are plotted as function of scattering energy *E*. (b) Three- and one-dimensional simulations of *ortho*-FH_2^- spectrum on 5SEC surface.

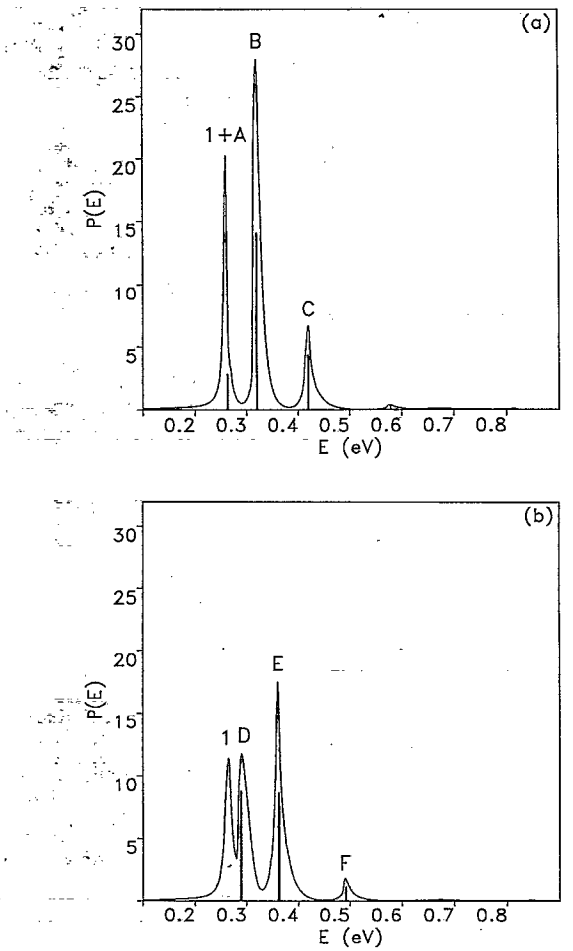

FIG. 7. (a) Three-dimensional simulations of *para*-FH_2^- spectrum on TS surface for F+H_2. One-dimensional simulation superimposed as stick spectrum. Scaling of the one-dimensional intensities is the same as in Fig. 6(a). (b) Three- and one-dimensional simulations of *ortho*-FH_2^- spectrum on TS surface.

sity. Note that peaks 1 and 2 are considerably narrower than the lettered peaks, suggesting that the corresponding scattering states are actually quasibound resonances.

A similar situation occurs in the TS simulation. The lowest energy peak, labeled peak 1+A in the *para* simulation and peak 1 in the *ortho* simulation, occurs at the same energy in both simulations. Peaks B and C appear only in the *para* simulation, while peaks D, E, and F appear only in the *ortho* simulation. This again suggests peaks B–F are due to progressions in bend/rotor levels of the FH_2 complex. The lowest energy peak lies just above the reactant zero-point energy. In simulations using the larger value of R_{F-H_2} in the anion (not shown), its intensity drops by about 70% in the *para* simulation and by more than 95% in the *ortho* simulation. This suggests that in the *para* simulation of Fig. 7(a), peak 1+A consists of overlapping transitions to a bend level of the F/H_2 complex (the A component) and a scattering state (the 1 component) localized on the product side of the saddle point; the A component of this peak is then absent in the *ortho* simulation.

In order to provide further support for these assignments, we have carried out one-dimensional simulations of the FH_2^- photoelectron spectrum in which only bending motion of the complex along the Jacobi angle γ is allowed. In these simulations, R_{F-H_2} and R_{H-H} on the neutral surface are fixed at their equilibrium values in the anion; only γ is allowed to vary. Hence, the one-dimensional simulation probe the bend potential of the neutral surface at the center of the Franck–Condon region.

The results of these simulations are superimposed on the three-dimensional simulations in Figs. 6 and 7. The one-dimensional simulations do an excellent job of reproducing the positions of the lettered peaks for both surfaces. Moreover, in the one-dimensional simulations, the appearance of peaks in the *para* vs *ortho* spectra mirrors the lettered peaks in the three-dimensional simulations. Peaks 1 and 2 do not appear in the one-dimensional 5SEC simulation, consistent with the notion that they are transitions to product scattering states. For the TS simulations, the relative intensity of peak 1+A is lower by about a third in the

TABLE II. Positions, widths, and assignments of peaks in *para* and *ortho* FH_2^- simulations on the 5SEC and TS surfaces [CCSD(T) anion geometry].

Simulation	Peak	Position/eV	FWHM/eV	Assignment
5SEC/*p*-FH_2^-				
	1	0.207	0.003	H/HF resonance
	2	0.280	0.001	H/HF resonance
	A	0.319	0.012	F/$H_2(j=0)$
	B	0.362	0.019	F/$H_2(2)$
	C	0.465	0.027	F/$H_2(4)$
5SEC/*o*-FH_2^-				
	1	0.207	0.003	H/HF resonance
	2	0.280	0.001	H/HF resonance
	D	0.329	0.016	F/$H_2(1)$
	E	0.405	0.019	F/$H_2(3)$
	F	0.538	0.032	F/$H_2(5)$
TS/*p*-FH_2^-				
	1	0.260	0.008	H/HF resonance
	+A			+F/$H_2(0)$
	B	0.318	0.014	F/$H_2(2)$
	C	0.417	0.010	F/$H_2(4)$
TS/*o*-FH_2^-				
	1	0.264	0.015	H/HF resonance
	D	0.289	0.022	F/$H_2(1)$
	E	0.358	0.010	F/$H_2(3)$
	F	0.491	0.014	F/$H_2(5)$

one-dimensional vs three-dimensional simulations, supporting the idea that it consists of two overlapping transitions.

Overall, the comparison between the two sets of simulations strongly supports the assignments of the lettered peaks to progressions in bend/rotor levels of the neutral complex. Moreover, the increasing spacing of these peaks with E suggests we are closer to the free rotor than rigid bender limit for the neutral complex (see Fig. 3). Hence, based on the energetic ordering of the peaks, each can be assigned to an F/$H_2(j)$ hindered rotor level which correlates asymptotically to the reactant free rotor level F+$H_2(j)$. These assignments are listed in Table II.

4. Comparison with experiment

Figures 8 and 9 show the *p*-FH_2^- and *n*-FH_2^- photoelectron spectra superimposed on appropriate simulations using the 5SEC and TS surfaces, respectively. The simulations have been convoluted with a 15 meV full width at half-maximum (FWHM) Gaussian to approximate the experimental resolution. Also, slightly different values of $D_0(FH_2^-)$ are used (0.20 and 0.24 eV for the 5SEC and TS simulations, respectively) to optimize the alignment of the simulated and experimental spectra; see Eqs. (1) and (2).

Both simulations of the *p*-FH_2^- spectra consist of a small number of peaks which approximately follow the contour of the experimental spectrum; it is difficult to choose which simulation is superior based on this comparison alone. However, the TS surface is clearly better with

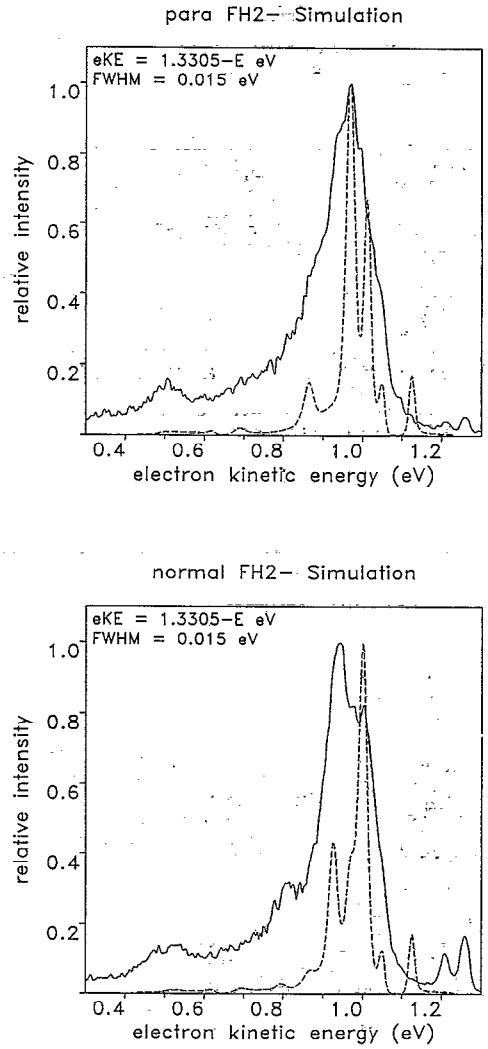

FIG. 8. Simulations of *p*-FH_2^- and *n*-FH_2^- photoelectron spectra using 5SEC surface superimposed on experimental ($\theta=0°$) spectra. $D_0=0.24$ eV is assumed for FH_2^- in the simulations.

respect to simulating the *n*-FH_2^- spectrum; the positions and intensities of the three main peaks in the experimental spectrum (A, A′, and B) are reproduced reasonably well in the TS simulation but not in the 5SEC simulation. Thus, the TS surface does better overall in simulating the FH_2^- photoelectron spectrum.

The reasonable agreement between the experimental spectra and TS simulations implies that most of the structure in the *experimental* spectra is due to progressions in bend/rotor levels of the FH_2 complex. This explains why some of the features in the *n*-FH_2^- spectrum are largely absent in the *p*-FH_2^- spectrum: transitions to both symmetric and antisymmetric bend/rotor levels occur in the *n*-FH_2^- spectrum, but only transitions to symmetric levels should occur in the *p*-FH_2^- spectrum. Based on the comparison with the TS simulations, the various peaks in the experimental spectrum can be assigned to transitions to F/$H_2(j)$ hindered rotor levels. Specifically, peak A′ can be assigned to the F/$H_2(j=2)$ level, while peaks A, B, and C, which are prominent only in the *n*-FH_2^- spectrum, are

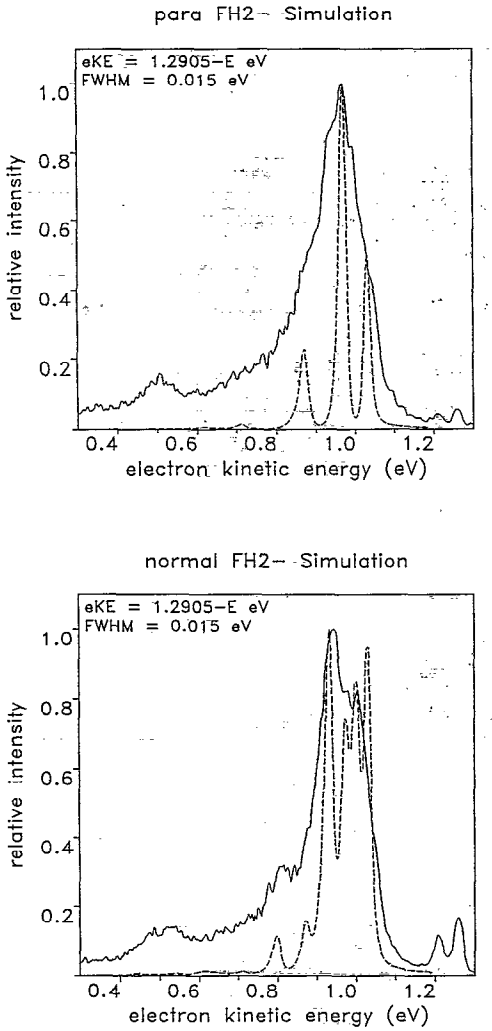

FIG. 9. Simulations of p-FH_2^- and n-FH_2^- photoelectron spectra using TS surface superimposed on experimental (θ=0°) spectra. D_0=0.20 eV is assumed for FH_2^- in the simulations.

due to F/H_2(j) levels with j=1, 3, and 5, respectively. The shoulder in the p-FH_2^- spectrum at 0.85 eV appears to be due to the F/H_2 (j=4) symmetric level.

Note that peaks A and B in the experimental spectra (see Fig. 2), although assigned to antisymmetric bend/rotor levels, are not completely gone in the p-FH_2^- spectrum. We believe this is because some H_2 *para*→*ortho* conversion takes place in the mixing cylinder prior to the experiment, so that there is some nonzero population of H_2 (j=odd) rotational levels in the reagent gas mixture. This is also at least part of the reason why the p-FH_2^- simulation is considerably more structured than the experimental spectrum. Another possible contribution to the discrepancy between experimental and simulated *para* spectra is that the peaks in the simulation are too narrow because of deficiencies in the TS surface; we have observed similar discrepancies in several past comparisons of experimental and simulated transition state photodetachment spectra where a LEPS surface is assumed to describe the reaction.[42]

In the n-FH_2^- simulation, the peak at highest electron kinetic energy is too intense. This is the sum of peak 1+A in Fig. 7(a) and peak 1 in Fig. 7(b) in a 1:3 ratio. In light of the discussion in Sec. 4C 3, most of the intensity of this peak is due to a scattering state localized on the product side of the saddle point. Its intensity would be reduced if the barrier height were increased, as this state would then have less amplitude in the Franck–Condon region, and hence less overlap with the anion wave function. This discrepancy thus points to a specific modification which should be made to the TS surface; the requirement of a higher barrier is consistent with the observation[12] that the transition state theory rate constant on the TS surface is too high.

We should emphasize that the center of the Franck–Condon region lies considerably closer to the collinear saddle point on the TS surface (for which R_{F-H_2} = 2.031 Å) than on the T5a surface (R_{F-H_2} = 1.953 Å). Hence, the overlap of the anion with the neutral transition state region is even better than in Fig. 1. This means that there should be very close correspondence between the peaks in the photoelectron spectrum and the bend/rotor levels of the F+H_2 transition state, assuming that the assignment implied by the comparison with the TS simulations is correct. On the other hand, the only peak in the TS simulations that might be due to a resonance, peak 1, is not clearly observable in the experimental spectrum at our current resolution.

Overall, the comparisons between the experimental and simulated spectra in Figs. 4, 8, and 9 show that the FH_2^- photoelectron spectrum is extremely sensitive to the nature of the bend potential in the transition state region. This seems to be approximately correct only on the TS surface. The bend potential is expected to play a major role in determining the reaction rate constant as well as the product energy and angular distributions. Hence, our experiment provides a very direct probe of one of the most important features of the F+H_2 potential energy surface.

Finally, we note that the FH_2^- photoelectron spectrum is qualitatively very different from our earlier studies[24] of heavy+light-heavy X+HY reactions via photoelectron spectroscopy of XHY^-. In the XHY^- studies, the most prominent features were progressions in the antisymmetric stretch mode of the XHY complex, although our higher resolution work on IHI^- did reveal structure attributable to bending/hindered rotor motion of the IHI complex.[63] These differences are understood in light of the internal coordinate along which the greatest change in the potential energy surface occurs upon photodetachment. In the XHY^- spectra, one typically has a single minimum potential along the antisymmetric stretch coordinate in the anion, and a double minimum potential in the neutral (in the center of the Franck–Condon region). In the case of FH_2^- photodetachment, the anion is a reasonably rigid linear species, while the bend potential for the neutral is a double minimum potential which is also considerably flatter than in the anion.

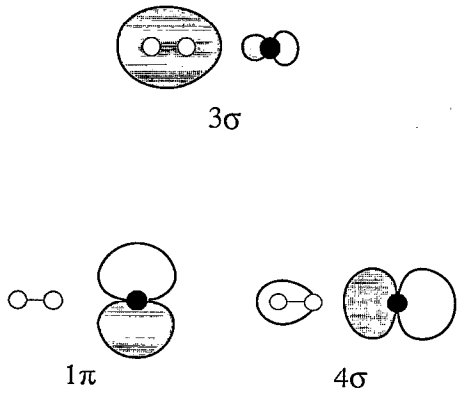

FIG. 10. Highest molecular orbitals for FH_2^-, showing the 3σ, one of the 1π, and the 4σ orbitals, all of which are fully occupied in the anion. The molecular orbitals are the optimized MP2/6-31++G** orbitals evaluated at the computed equilibrium structure for the FH_2^- ion at the same level of *ab initio* theory.

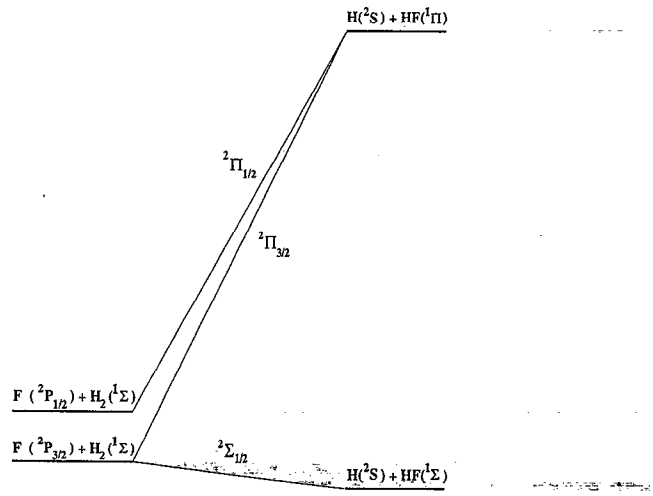

FIG. 11. Electronic correlation diagram for F+H_2.

D. Electronic effects

In this section, we consider what can be learned about the low-lying excited state F+H_2 potential energy surfaces from the broad features at low electron kinetic energy in the $\theta=90°$ spectra of Fig. 2.

1. Background

The approach of a F atom with a ground state H_2 molecule may occur on three potential energy surfaces, which are labeled 1 ^{2}A′, ^{2}A″, and 2 ^{2}A′ in the most general symmetry of collision (C_s). The upper ^{2}A″ and 2 ^{2}A′ surfaces become degenerate in $C_{\infty v}$ (collinear approach) so that there are only two surfaces $^2\Sigma$ and $^2\Pi$. Figure 10 shows the highest occupied molecular orbitals for the anion, where the $C_{\infty v}$ point group is appropriate. Photodetachment of an electron from the filled 4σ and 1π orbitals leads to the $^2\Sigma$ and $^2\Pi$ states, respectively, in the neutral. Only the lowest surface, the $^2\Sigma$, where the fluorine atom approaches with the p orbital containing the unpaired electron along the H_2 bond, adiabatically leads to reaction. It is this ground state surface that we have focused on in the preceding sections. The introduction of spin orbit coupling in the F atom splits the degeneracy of the upper $^2\Pi$ surfaces in $C_{\infty v}$ and the correct state labels are $^2\Sigma_{1/2}$, $^2\Pi_{3/2}$, and $^2\Pi_{1/2}$. The $^2P_{3/2}$–$^2P_{1/2}$ splitting in the fluorine atom is 0.0501 eV.[64] A correlation diagram is shown in Fig. 11. In the adiabatic limit, only the $^2\Sigma_{1/2}$ surface leads to H+HF reaction products and the F($^2P_{1/2}$) state is completely unreactive. However, reaction may also take place via the $^2\Pi_{1/2}$ surface if nonadiabatic coupling is appreciable.

A number of model potential energy surfaces have been proposed for the excited state surfaces over the years. In 1972, Blais and Truhlar constructed semiempirical valence bond surfaces for the $^2\Sigma$ and $^2\Pi$ states.[65] An *ab initio* calculation of these surfaces at the SCF level was subsequently carried out by Rebentrost and Lester.[66] Spin–orbit effects were neglected in these studies, but were included semiempirically in the calculation of collinear and three-dimensional surfaces by Jaffe *et al.*[67] and Komornicki *et al.*[32] and in diatomics-in-molecules (DIM) calculations by Tully,[31] and by Faist and Muckerman.[33] The effect of the excited states on the FHH bend potential on the ground state surface has been considered recently by Wright.[68]

Several of these studies have considered the reactivity of the F($^2P_{1/2}$) state via nonadiabatic effects. Semiclassical scattering calculations by Tully,[31] Komornicki,[32] and Muckerman[33] demonstrated that the F($^2P_{1/2}$)+H_2 may contribute significantly to the overall reaction cross section. The multisurface problem was also considered in collinear quantal scattering calculations by Zimmerman *et al.*[34] and LePetit *et al.*[35] The other nonadiabatic effect of interest is electronic-to-rotational energy transfer since the spin–orbit splitting in F is very close to the $j=0-2$ spacing in H_2. This process has been predicted to be quite efficient in calculations by Rebentrost[36] and Wyatt.[37]

One point that emerges from these studies, not surprisingly, is that the reactivity of the F($^2P_{1/2}$) state depends strongly on the assumed form of the ground and excited state surfaces used in the scattering calculations, and the excited state surfaces are particularly suspect. The *ab initio* calculation of excited state surfaces is a challenge, and, until recently, there has been very little experimental data to aid in the empirical development of these surfaces. Experiments on the F+H_2 reaction by Lee and co-workers[4] showed no evidence for reactivity of F($^2P_{1/2}$), nor did the experiments of Hepburn *et al.* on the F+HBr reaction, for which one might expect similar nonadiabatic effects in the entrance channel as in the F+H_2 reaction.[69] The experimental work most directly related to the excited states has been performed by Aquilanti and co-workers.[38] By measuring the total scattering cross section of magnetically analyzed F atoms with D_2 as a function of collision energy, they reported experimentally determined potentials for all three states. However, only the long range part of each potential ($R_{F-H_2} > 2.5$ Å) is well characterized in these experiments, although their derived functional forms for the potentials can be extrapolated to shorter range.

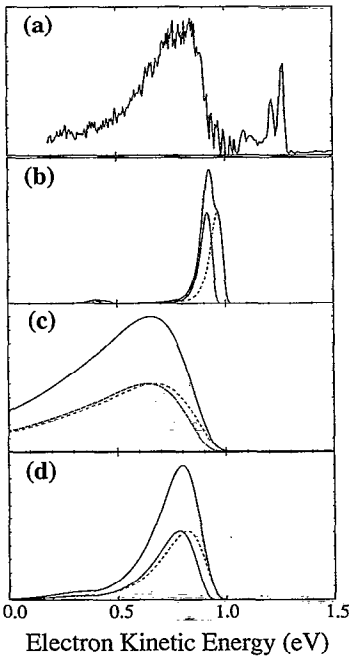

FIG. 12. (a) Difference plot of the 266 nm *normal*-FH_2^- spectra. Here the $\theta=0°$ spectrum has been scaled and subtracted from the $\theta=90°$ spectrum to yield the band due to transitions from the anion to the $^2\Pi_{3/2}$ and $^2\Pi_{1/2}$ FH_2 states. (b)–(d) Collinear two-dimensional simulations of the $^2\Pi$ bands described in text. Potential along R_{F,H_2} constructed as follows: (b) V_{rep} chosen to approximate DIM curves of Ref. 31, (c) from functional form and parameters from Ref. 38, and (d) V_{rep} chosen to yield a fit to photoelectron band (a). In all simulations, transitions to both spin orbit components of the $^2\Pi$ state have been considered, and are assumed to have equal transition probability (dashed and dot-dashed lines). The sum of the two subbands are shown by the solid line.

As mentioned above, photodetachment of FH_2^- accesses both the ground and excited state F+H_2 surfaces. Our photoelectron spectra probe these surfaces at closer range than Aquilanti's work and therefore provide complementary information on the potentials. In the following sections, we first describe how the contribution of the excited states to the FH_2^- photoelectron spectrum in Fig. 2 is determined. We then present simulations of the spectrum on various excited state potentials.

2. Extraction of excited state bands

As discussed in Sec. 4A and in our previous work,[27] the contribution of the $^2\Pi$ states to the FH_2^- photoelectron spectrum is all but eliminated at the laser polarization angle $\theta=0°$. This spectrum may then be used as a reference spectrum for the $^2\Sigma$ band, and we may subtract this spectrum, appropriately scaled, from the $\theta=90°$ spectrum to determine the contribution of the $^2\Pi$ states. Let us assume that feature A (at highest eKE) in the *normal*-FH_2^- spectrum has no contribution from the excited electronic states, and so this peak is a marker of the contribution of the $^2\Sigma_{1/2}$ surface to the photoelectron spectrum for the scaling procedure in the subtraction.

Figure 12(a) shows the subtracted result which we will assume represents the spectrum of transitions from the anion to the $^2\Pi_{3/2,1/2}$ states only. The two photon F^- peaks at 1.21 and 1.26 eV appear with relatively large intensity in the difference plot because the $F(^2P_{3/2,1/2})\leftarrow F^-$ transitions also have electron angular distributions peaked at $\theta=90°$. The noise in the region 0.9–1.1 eV is most likely due to slight differences in the $^2\Sigma$ band shape due to incomplete signal averaging, which is amplified in the subtraction process. The structure we are interested in lies between 0.5 and 0.9 eV. The band rises fairly sharply at eKE=0.9 eV, peaks at approximately 0.8 eV, and has a FWHM of ~0.3 eV. We note that the band is quite asymmetrical.

In order to ensure that the spectrum in Fig. 12(a) represents the entire $^2\Pi$ band, we have recorded photoelectron spectra of *normal*-FH_2^- at 213 nm (not shown), where the photon energy is 1.17 eV higher. The spectra are essentially identical to their respective 266 nm counterparts, except for the 1.17 eV shift to higher eKE and diminished spectral resolution. The polarization dependence of the signal is also the same. The important result is that no additional bands are observed for FH_2^- photodetachment that are not present in the 266 nm spectra. Thus, there are no other electronic bands within 2 eV of the $^2\Sigma$ band except those seen in the 266 nm spectrum appearing at polarization $\theta=90°$. Further, Muckerman's semiquantitative correlation diagram predicts that only one electronic state, the $^2\Pi$ state, is expected within 6 eV of the ground state.[33] Hence we may confidently assume that the allowed transitions from the anion to both the $^2\Pi_i$ components are those in the 266 nm spectrum between eKE=0.5 and 0.9 eV.

3. $^2\Pi$ simulations

As described above, several potential energy curves have been proposed for the Π interaction between F and H_2. The potentials are essentially repulsive as they correlate to high lying, dissociative, states of HF (see Fig. 10). To assess the accuracy of these curves in the Franck–Condon region, we attempt to simulate the photoelectron band in Fig. 12(a) using two of these potentials: the diatomics-in-molecules (DIM) potentials of Tully[31] and the experimentally derived potentials of Aquilanti *et al.*[38]

Since the excited state curves are strongly repulsive along the R_{F-H_2} coordinate, the photoelectron spectrum is largely determined by the slopes of these curves in the Franck–Condon region, and effects due to differences between the bend potentials of the anion and neutral should be relatively minor. We therefore restrict the simulations to collinear geometries, and use two-dimensional potential energy surfaces of the form

$$V_{\Pi}^{(i)}=V_{\text{bound}}(R_{H-H})+V_{\text{rep}}^{(i)}(R_{F,H_2}), \tag{3}$$

where V_{bound} is the bound $^1\Sigma_g^+$ potential curve of H_2, modeled by a Morse function, $V_{\text{rep}}^{(i)}$ is the repulsive interaction of the F atom with H_2 in a Π configuration and $i=3/2$, 1/2.

Tully calculated V_{rep} for both spin orbit components.[31] The resultant DIM potentials can be approximately described by exponential functions,

$$V_{\text{rep}}^{(3/2)}=A_{3/2}\exp(-\beta_{3/2}R_{F,H_2}),$$
$$V_{\text{rep}}^{(1/2)}=A_{1/2}\exp(-\beta_{1/2}R_{F,H_2})+\Delta, \quad (4)$$

where $\Delta=0.0501$ eV, the spin–orbit splitting in fluorine,[64] and V is in units of eV and R_{F,H_2} in Å. In contrast, the experimentally fitted V_{rep} potential curves of Aquilanti *et al.*[38] are formulated using a more complex functional form, which can be evaluated at the shorter values of R_{F,H_2} in the Franck–Condon region in order to simulate the spectrum.

To simulate the photoelectron band, we need to calculate the overlap of the anion ground state wavefunction with the scattering states supported by each $^2\Pi$ surface. If we ignore nonadiabatic effects, as also assumed in the ground state simulations in Sec. IV C, a relatively simple quantum mechanical calculation using the potential function given by Eq. (3) will yield the scattering states for each spin–orbit surface. We actually simulate the excited state spectrum with a two-dimensional wave-packet propagation calculation.[70] This is formally equivalent to the time-independent methods used in the previous section, although the dimensionality of the time-dependent calculation is lower. The contribution of the $^2\Pi$ states, and the model we are using to describe it, is very similar to the that of the F+HO→HF+O(^{1}D) reaction to the OHF^- spectrum.[71] In the Franck–Condon region the V_Π potentials are fairly repulsive, so the wave packet moves quickly out of this region, and only a short propagation time is necessary. All the $^2\Pi$ simulations assume the *ab initio* anion geometry and frequencies of Nichols *et al.*[25] In contrast to the ground state simulations, a Morse potential (rather than a harmonic potential) is assumed for the H–H stretch in the anion with $\omega_e x_e$ (but not r_e) the same as in free H_2.[72] A value of $D_0=0.23$ eV was assumed for the anion dissociation energy [see Eq. (44)]. For the V_{bound} term in V_Π, Morse parameters derived from the spectroscopic constants of H_2 are used.

The first simulation [Fig. 12(b)] assumes $\beta_{3/2}=5.53$ Å^{-1}, $A_{3/2}=3022$ eV, $\beta_{1/2}=5.60$ Å^{-1}, and $A_{1/2}=2950$ eV for V_{rep} in Eq. (4); these parameters give the best fit to the DIM potential curves shown in Fig. 2 of Ref. 31. Each subband has similar shape and the shape reproduces the experimental band shape in that it rises fairly rapidly at lower scattering energies (high eKE) and has a longer tail at low eKE. However, it is immediately apparent that V_{rep} is not repulsive enough to reproduce the FWHM of the band. The FWHM in the simulation, for each $^2\Pi$ component, is only 0.065 eV. Further, the onset of the band (the high eKE edge) is very close to the F+H_2(v=0) asymptote near 1 eV, and in comparison to the experimental band is at too high electron kinetic energy.

The simulation in Fig. 12(c) results from using the much more repulsive excited state potentials of Aquilanti for $V_{\text{rep}}^{(i)}$. The simulated band onset is at much lower eKE (0.75 eV) and the band has a much wider FWHM, 0.62 eV, than the simulations on the DIM-like potentials. This is clearly at the opposite extreme; the surface is now too repulsive at the calculated anion geometry. We note in passing that the potential of Blais and Truhlar,[65] which has been used by others in dynamical studies,[34,35] although less repulsive than that of Aquilanti, also yields a simulated band much wider than experimentally observed.

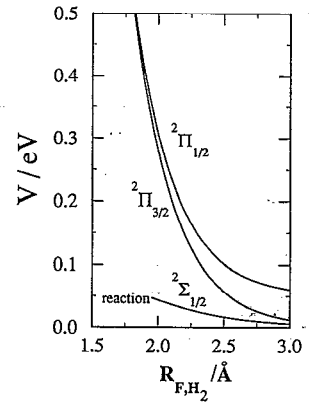

FIG. 13. The variation of potential energy for the three lowest lying electronic states of FH_2 as a function of the F to H_2 distance. Lowest curve ($^2\Sigma_{1/2}$) is calculated from the T5a surface (Ref. 10), upper $^2\Pi_{3/2,1/2}$ surfaces are those calculated to best fit difference spectrum Fig. 12(d) (see the text). The $^2\Sigma_{1/2}$ curve is included only for purposes of comparison; it was not used in the simulations in Fig. 12.

The third simulation shown, Fig. 12(d), is a compromise "fit." Here we have again used a V_{rep} with the form of Eq. (4), but, compared to that used in the first simulation, the fit potential has the correct slope and potential energy offset at the anion F to H_2 separation. The fitted V_{rep} curves ($\beta_{3/2}=3.18$ Å^{-1}, $A_{3/2}=161.5$ eV, $\beta_{1/2}=3.22$ Å^{-1}, $A_{1/2}=161.9$ eV) are shown in Fig. 13 along with the T5a potential for the $^2\Sigma$ state. The vertical energy differences from the $^2\Sigma_{1/2}$ to the $^2\Pi_{3/2}$ and $^2\Pi_{1/2}$ curves in Fig. 13 at the anion R_{F,H_2} are 0.18 and 0.21 eV. In comparison, Simons' *ab initio* calculation suggested 0.25 eV for the $^2\Sigma$–$^2\Pi$ splitting at this geometry,[25] whereas Tully's DIM curves suggest 0.01 and 0.06 eV separation from the $^2\Sigma_{1/2}$ to the $^2\Pi_{3/2}$ and $^2\Pi_{1/2}$, respectively.[31] Wright gives the $^2\Sigma$–$^2\Pi$ separation at the Σ state saddle point geometry as ~0.78 eV.[68] The simulated subbands in Fig. 12(d) are separated by 0.03 eV at the band maximum and the FWHM for the $^2\Pi_{3/2}$ and $^2\Pi_{1/2}$ subbands are 0.23 and 0.21 eV, respectively. The sum of the simulated subbands approximately reproduces the whole unresolved band in our experimental spectrum.

The small bump observable at low electron kinetic energies (0.3–0.4 eV) in simulations (b) and (d) (in each spin orbit component) is due to overlap with states correlating to H_2 (v=1); there is overlap to these vibrationally excited states because the anion has a slightly elongated H–H bond, and the valleys in the V_Π surfaces have R_{H-H} set at the equilibrium H_2 value. The intensity of this band depends on two factors, the degree of H–H elongation in the anion and on the anharmonicity assumed along the H–H stretch in the anion. It seems reasonable to expect $\omega_e x_e$ for this mode to be at least as large in the anion as it is for free H_2, which we have assumed in the simulation, and it is most likely larger (which would yield more intensity in the v=1 bump). This may account for some of the

signal extending out to low eKEs in the experimental difference plot.

The important result here is that the $^2\Pi$ surfaces rise more steeply in the interaction region than predicted by the DIM approach, but less steeply than extrapolated by Aquilanti's potentials fitted to low energy elastic scattering data. We have therefore determined improved potential parameters for V_{rep} at short range, with the caveat that the CCSD(T) *ab initio* value of Nichols for the anion equilibrium geometry, used throughout this paper, has been assumed to be correct. The simulated bandwidth is, unfortunately, strongly dependent on the assumed anion equilibrium R_{F,H_2}. Assuming the *ab initio* anion geometry is reasonably accurate, then our results for the Π potentials indicate that there is stronger nonadiabatic coupling between the $\Omega=1/2$ surfaces near the ground state saddle point than one would suppose based on Aquilanti's potentials. However, it remains to be seen if these nonadiabatic effects are sufficiently strong to noticeably influence the reaction dynamics.

V. SUMMARY

In this work we have presented new experimental and theoretical results on the spectroscopy of the $F+H_2$ transition via photodetachment of FH_2^-. The experimental FH_2^- photoelectron spectra show transitions to the ground $F+H_2$ potential energy surface as well as to low-lying excited state surfaces. There are pronounced differences in the ground state photoelectron band depending on whether the FH_2^- is synthesized from *normal* or *para* hydrogen. These differences indicate that previous comparisons of the *n*-FH_2^- photoelectron spectrum with theory were, in retrospect, inappropriate. The striking dependence on the nuclear spin statistics in the anion is interpreted to mean that the photoelectron spectra consist of progressions in bend/hindered rotor levels of the FH_2 complex. This interpretation is strongly supported by one- and three-dimensional simulations of the *para* and *normal* photoelectron spectra performed on several different surfaces for the $F+H_2$ reaction. These simulations explicitly account for the anion nuclear spin statistics. The best agreement in the work reported here is obtained with the empirical TS surface from Ref. 12; the agreement between the experimental and simulated spectra is considerably better than when either the T5a or 5SEC surface is used.

Quantitative consideration of the excited state bands, assigned to the $^2\Pi_{3/2}$ and $^2\Pi_{1/2}$ states, has been made here, and collinear simulations have allowed the determination of the shape of these potential curves along the R_{F,H_2} coordinate. These results represent the first experimental characterization of the excited state potentials at geometries close to the transition state on the ground state surface. We hope that the results of this analysis will stimulate new *ab initio* work on characterizing these excited state surfaces, and their nonadiabatic coupling to the ground state surface.

There is clearly much still to learn about the $F+H_2$ reaction, and our photoelectron experiments have introduced a new experimental approach into the fitting of the potential surfaces, both in the transition state region for the ground reaction surface and in the inner regions of the upper nonreactive surfaces. Further experiments to extract even more detail are possible. Zero electron kinetic energy (ZEKE) photodetachment spectroscopy, with an attainable resolution of 2–3 cm^{-1}, would be particularly useful for this transition state system.[63,73] As the feature A in the *normal*-FH_2^- spectrum is quite narrow, a more concrete assignment of the FH_2^- internal states giving rise to the peaks in this region should be possible in a ZEKE spectrum.

On the theoretical side, new simulations for the photoelectron spectrum of FD_2^- have been performed on the surfaces considered here and will be published elsewhere.[74] These support the current bending assignments when compared to the experimental FD_2^- spectrum.[27] Also, Werner and co-workers[75] have recently developed a new *ab initio* $F+H_2$ surface, and preliminary simulations of the *p*-FH_2^- and *n*-FH_2^- photoelectron spectra yield even better agreement with the experimental spectra than in the results reported here.[76] Moreover, Simons[49] has performed *ab initio* calculations on more of the FH_2^- potential energy surface. This will enable the determination of more realistic anion vibrational wave functions than the harmonic wave functions used in the simulations reported here. It should therefore be possible to perform very stringent tests of this new surface in the near future.

ACKNOWLEDGMENTS

We would like to thank Professor J. Zhang for communicating new Franck–Condon results for the 5SEC surface. We thank Professor R. J. Saykally for useful discussions on nuclear spin statistics considerations in the FH_2^- anion. This work has been sponsored by the United States Air Force Office of Scientific Research under Contract No. AFOSR-91-0084, and by the United Kingdom Science and Engineering Research Council.

[1] J. H. Parker and G. C. Pimentel, J. Chem. Phys. **51**, 91 (1969); R. D. Coombe and G. C. Pimentel, *ibid.* **59**, 251 (1973); M. J. Berry, *ibid.* **59**, 6229 (1973).
[2] J. C. Polanyi and D. C. Tardy, J. Chem. Phys. **51**, 5717 (1969); J. C. Polanyi and K. B. Woodall, *ibid.* **57**, 1574 (1972); N. Jonathan, C. M. Melliar-Smith, and D. H. Slater, Mol. Phys. **20**, 93 (1971).
[3] T. P. Schafer, P. E. Siska, J. M. Parson, F. P. Tully, Y. C. Wong, and Y. T. Lee, J. Chem. Phys. **53**, 3385 (1970).
[4] D. M. Neumark, A. M. Wodtke, G. N. Robinson, C. C. Hayden, and Y. T. Lee, J. Chem. Phys. **82**, 3045 (1985); D. M. Neumark *et al.*, *ibid.* **82**, 3067 (1985).
[5] M. Faubel, S. Schlemmer, F. Sondermann, and J. P. Toennies, J. Chem. Phys. **94**, 4676 (1991).
[6] E. Wurzburg and P. L. Houston, J. Chem. Phys. **72**, 4811 (1980); R. F. Heidner, J. F. Bott, C. E. Gardner, and J. E. Melzer, *ibid.* **72**, 4815 (1980).
[7] W. H. Miller, Annu. Rev. Phys. Chem. **41**, 245 (1990).
[8] C. F. Bender, P.K. Pearson, S. V. O'Neill, and H. F. Schaeffer, J. Chem. Phys. **56**, 4626 (1972); Science **176**, 1412 (1972); H. F. Schaeffer, J. Phys. Chem. **89**, 5336 (1985).
[9] J. T. Muckerman, in *Theoretical Chemistry-Advances and Perspectives*, edited by H. Eyring and D. Henderson (Academic, New York, 1981), Vol. 6A, pp. 1–77.
[10] R. Steckler, D. G. Truhlar, and B. C. Garrett, J. Chem. Phys. **82**, 5499 (1985).

[11] G.C. Lynch, R. Steckler, D. W. Schwenke, A. J. C. Varandas, and D. G. Truhlar, J. Chem. Phys. **94**, 7136 (1991).
[12] T.Takayanagi and S. Sato, Chem. Phys. Lett. **144**, 191 (1988).
[13] C. W. Bauschlicher, S. P. Walch, S. R. Langhoff, P. R. Taylor, and R. L. Jaffe, J. Chem. Phys. **88**, 1743 (1988); R. J. Bartlett, J. Phys. Chem. **93**, 1697 (1989).
[14] D. G. Truhlar, J. Chem. Phys. **56**, 3189 (1972); J. T. Muckerman and M. D. Newton, *ibid.* **56**, 3191 (1972).
[15] G. C. Schatz, J. M. Bowman, and A. Kuppermann, J. Chem. Phys. **63**, 674 (1975); J. N. L. Connor, W. Jakubetz, and J. Manz, Mol. Phys. **35**, 1301 (1978); R. E. Wyatt, J. F. McNutt, and M. J. Redmon, Ber. Bunsenges Phys. Chem. **86**, 437 (1982).
[16] J. D. Kress, Z. Bacic, G. A. Parker, and R. T Pack, Chem. Phys. Lett. **157**, 484 (1989); Z. Bacic, J. D. Kress, G. A. Parker, and R. T Pack, J. Chem. Phys. **92**, 2344 (1990).
[17] C.-H. Yu, D. J. Kouri, M. Zhao, and D. G. Truhlar, Chem. Phys. Lett. **157**, 491 (1989); C.-H. Yu, D. J. Kouri, M. Zhao, D. G. Truhlar, and D. W. Schwenke, Int. J. Quantum Chem. **23**, 45 (1989).
[18] J. Z. H. Zhang and W. H. Miller, J. Chem. Phys. **92**, 1811 (1990).
[19] D. E. Manolopoulos, M. D'Mello, and R. E. Wyatt, J. Chem. Phys. **93**, 403 (1990); M. D'Mello, D. E. Manolopoulos, and R. E. Wyatt, Chem. Phys. Lett. **168**, 113 (1990).
[20] (a) J. M. Launay and M. LeDourneuf, Chem. Phys. Lett. **169**, 473 (1990); (b) J. M. Launay, Theor. Chim. Acta **79**, 183 (1990).
[21] G. C. Lynch *et al.*, J. Chem. Phys. **94**, 7150 (1991).
[22] J. D. Kress and E. F. Hayes, J. Chem. Phys. **97**, 4881 (1992).
[23] F. J. Aoiz, V. J. Herrero, M. M. Nogueira, and V. Saez Rabanos, Chem. Phys. Lett. **204**, 359 (1993).
[24] R. B. Metz, S. E. Bradforth, and D. M. Neumark, Adv. Chem. Phys. **81**, 1 (1992).
[25] J. A. Nichols, R. A. Kendall, S. J. Cole, and J. Simons, J. Phys. Chem. **95**, 1074 (1991).
[26] A. Weaver, R. B. Metz, S. E. Bradforth, and D. M. Neumark, J. Chem. Phys. **93**, 5352 (1990).
[27] A. Weaver and D. M. Neumark, Faraday Discuss. Chem. Soc. **91**, 5 (1991).
[28] J. Z. H. Zhang, W. H. Miller, A. Weaver, and D. M. Neumark, Chem. Phys. Lett. **182**, 283 (1991).
[29] O. Hahn and H. S. Taylor, J. Chem. Phys. **96**, 5915 (1992).
[30] E. Pollak, M. S. Child, and P. Pechukas, J. Chem. Phys. **72**, 1669 (1980); E. Pollak, Chem. Phys. **61**, 305 (1981).
[31] J. C. Tully, J. Chem. Phys. **59**, 5122 (1973); **60**, 3042 (1974).
[32] A. Komornicki, K. Morokuma, and T. F. George, J. Chem. Phys. **67**, 5012 (1977).
[33] M. B. Faist and J. T. Muckerman, J. Chem. Phys. **71**, 233 (1978).
[34] I. H. Zimmerman, M. Baer, and T. F. George, J. Chem. Phys. **71**, 4132 (1979).
[35] B. LePetit, J. M. Launay, and M. Le Dourneuf, Chem. Phys. **106**, 111 (1986).
[36] F. Rebentrost and W. A. Lester, J. Chem. Phys. **67**, 3367 (1977).
[37] R. E. Wyatt and R. B. Walker, J. Chem. Phys. **70**, 1501 (1979).
[38] V. Aquilanti, R. Candori, D. Cappelletti, E. Luzzatti, and F. Pirani, Chem. Phys. **145**, 293 (1990).
[39] D. Proch and T. Trickl, Rev. Sci. Instrum. **60**, 713 (1989).
[40] J. E. Pollard, D. J. Trevor, J. E. Reutt, Y. T. Lee, and D. A. Shirley, J. Chem. Phys. **77**, 34 (1982).
[41] R. E. Continetti, Ph.D. thesis, University of California, Berkeley (1989).
[42] R. B. Metz, A. Weaver, S. E. Bradforth, T. N. Kitsopoulos, and D. M. Neumark, J. Phys. Chem. **94**, 1377 (1990).
[43] H. Hotop and W. C. Lineberger, J. Phys. Chem. Ref. Data **14**, 731 (1985).
[44] The peak labeling scheme of Refs. 27 and 28 is also used here to avoid confusion.
[45] C. Blondel, P. Cacciani, C. Delsart, and R. Trainham, Phys. Rev. A **40**, 3698 (1989).
[46] The equilibrium structure of FH_2^- is assumed to be linear on the basis of *ab initio* calculations of Simons (Ref. 25). A linear structure is consistent with the electrostatic forces of a charge interacting with the H_2 quadrupole moment.
[47] G. Henderson and G. E. Ewing, J. Chem. Phys. **59**, 2280 (1973); Mol. Phys. **27**, 903 (1974).
[48] The calculations compare the energy at the MP2/6-31++G** optimized linear geometry, which is close to Nichols', CCSD geometry, (Ref. 25) and the energy for the rotated configuration (C_{2v}) with R_{F,H_2} and R_{H-H} held constant. The calculated barrier is approximately invariant to the level of correlation correction to the energy. RHF, RMP2, and RMP4(SDQ) all give about the same barrier to internal rotation.
[49] J. Simons (private communication).
[50] G. C. Schatz, J. Chem. Phys. **90**, 3582 (1990).
[51] G. C. Schatz, J. Chem. Phys. **90**, 4847 (1990).
[52] G. C. Schatz, J. Phys. Chem. **94**, 6157 (1990).
[53] G. C. Schatz, Chem. Phys. Lett. **150**, 92 (1988).
[54] Y. B. Band, K. F. Freed, and D. J. Kouri, J. Chem. Phys. **74**, 4380 (1981).
[55] D. E. Manolopoulos, J. Chem. Phys. **85**, 6425 (1986).
[56] D. E. Manolopoulos, M. J. Jamieson, and A. D. Pradhan, J. Comput. Phys. **105**, 169 (1993).
[57] The anion parameters used by Zhang *et al.* were the following: $R_{F,H_2}=2.138$ Å; $R_{H-H}=0.796$ Å, and harmonic frequencies $\omega_1=302$ cm^{-1}, $\omega_2=693$ cm^{-1}, and $\omega_3=3816$ cm^{-1}. These values changed slightly in the final version of Ref. 25.
[58] J. Z. H. Zhang and W. H. Miller, J. Chem. Phys. **88**, 4549 (1988).
[59] T5a simulations using the published CCSD(T) anion *ab initio* equilibrium geometry and MCSCF harmonic frequencies show only small differences with the simulations displayed here.
[60] F. B. Brown and D. G. Truhlar, Chem. Phys. Lett. **117**, 307 (1985).
[61] S. Sato, Bull. Chem. Soc. Jpn. **28**, 450 (1955).
[62] D. C. Chatfield, R. S. Friedman, D. G. Truhlar, B. C. Garrett, and D. W. Schwenke, J. Am. Chem. Soc. **113**, 486 (1991); J. M. Bowman, Chem. Phys. Lett. **141**, 545 (1987).
[63] I. M. Waller, T. N. Kitsopoulos, and D. M. Neumark, J. Phys. Chem. **94**, 2240 (1990).
[64] S. Baskin and J. O. Stoner, Jr., *Atomic Energy Level and Grotian Diagrams* (North-Holland, New York, 1978), Vol. 1.
[65] N. C. Blais and D. G. Truhlar, J. Chem. Phys. **58**, 1090 (1973).
[66] F. Rebentrost and W. A. Lester, Jr., J. Chem. Phys. **63**, 3884 (1976).
[67] R. L. Jaffe, K. Morokuma, and T. F. George, J. Chem. Phys. **63**, 3417 (1975).
[68] M. Kolbuszewski and J. S. Wright, J. Chem. Phys. **96**, 5548 (1992).
[69] J. W. Hepburn, K. Liu, R. G. MacDonald, F. J. Northrup, and J. C. Polanyi, J. Chem. Phys. **75**, 3353 (1981).
[70] S. E. Bradforth, A. Weaver, D. W. Arnold, R. B. Metz, and D. M. Neumark, J. Chem. Phys. **92**, 7205 (1990).
[71] S. E. Bradforth, D. W. Arnold, R. B. Metz, A. Weaver, and D. M. Neumark, J. Phys. Chem. **95**, 8066 (1991).
[72] K. P. Huber and G. Herzberg, *Spectra of Diatomic Molecules* (Van Nostrand Reinhold, New York, 1979), Vol. IV.
[73] K. Muller-Dethlefs, M. Sander, and E. W. Schlag, Z. Naturforsch. Teil A **39**, 1089 (1984); T. N. Kitsopoulos, I. M. Waller, J. G. Loeser, and D. M. Neumark, Chem. Phys. Lett. **159**, 300 (1989).
[74] D. E. Manolopoulos (unpublished).
[75] H.-J. Werner (private communication).
[76] D. E. Manolopoulos, K. Stark, H.-J. Werner, D. W. Arnold, S. E. Bradforth, and D. M. Neumark, Science (submitted).